Published in final edited form as:

Prostate Cancer Imaging (2011). 2011 ; 6363: 100–108.

A PET/CT Directed, 3D Ultrasound-Guided Biopsy System for Prostate Cancer

Baowei Fei[1,2,5], **Viraj Master**[3], **Peter Nieh**[3], **Hamed Akbari**[1], **Xiaofeng Yang**[1], **Aaron Fenster**[4], and **David Schuster**[1]

Baowei Fei: bfei@emory.edu

[1]Department of Radiology and Imaging Sciences, Emory University, Atlanta, GA 30329

[2]Winship Cancer Institute, Emory University, Atlanta, GA 30329

[3]Department of Urology, Emory University, Atlanta, GA 30329

[4]Imaging Research Laboratories, Robarts Research Institute, London, Ontario, Canada, N6A 5K8

[5]Department of Biomedical Engineering, Emory University and Georgia Institute of Technology, Atlanta, GA 30329

Abstract

Prostate cancer affects 1 in 6 men in the USA. Systematic transrectal ultrasound (TRUS)-guided biopsy is the standard method for a definitive diagnosis of prostate cancer. However, this *"blind"* biopsy approach can miss at least 20% of prostate cancers. In this study, we are developing a PET/CT directed, 3D ultrasound image-guided biopsy system for improved detection of prostate cancer. In order to plan biopsy in three dimensions, we developed an automatic segmentation method based wavelet transform for 3D TRUS images of the prostate. The segmentation was tested in five patients with a DICE overlap ratio of more than 91%. In order to incorporate PET/CT images into ultrasound-guided biopsy, we developed a nonrigid registration algorithm for TRUS and PET/CT images. The registration method has been tested in a prostate phantom with a target registration error (TRE) of less than 0.4 mm. The segmentation and registration methods are two key components of the multimodality molecular image-guided biopsy system.

Keywords

Molecular imaging; PET/CT; image segmentation; nonrigid image registration; wavelet transform; 3D ultrasound imaging; prostate cancer; image-guided biopsy

1 Introduction

Systematic transrectal ultrasound (TRUS)-guided prostate biopsy is considered as the standard method for prostate cancer detection. The current biopsy technique has a significant sampling error and can miss at least 20% of cancers [1]. As a result, a patient may be informed of a negative biopsy result but may in fact be harboring an occult early-stage

Correspondence to: Baowei Fei, bfei@emory.edu.

cancer. It is a difficult challenge for physicians to manage patients with false negative biopsies who, in fact, harbor curable prostate cancer as indicated by biochemical measurements such as rising prostate specific antigen (PSA), as well as patients diagnosed with early-stage disease.

Although ultrasound imaging is a preferred method for image-guided biopsy because it is performed in real time and because it is portable and cost effective, current ultrasound imaging technology has difficulty to differentiate carcinoma from benign prostate tissue. MR spectroscopic imaging (MRSI) is playing an increasing role in prostate cancer management [2–3]. Various PET imaging agents have been developed for prostate cancer detection and staging, these include ^{18}F-FDG [4], ^{11}C-choline [5], ^{18}F-fluorocholine [6], ^{11}C-acetate [7], ^{11}C-methionine [8], and other PET agents. ^{18}F-FDG is widely used in cancer applications. However, it has low sensitivity in the primary staging of prostate cancer and poor detection of abdominal-pelvic nodes because of excretion of tracers in the ureters, bladder, and bowel. PET imaging with new molecular imaging tracers such as FACBC has shown promising results for detecting and localizing prostate cancer in humans [9]. FACBC PET images show focal uptake at the tumor and thus could be ideal information to direct targeted biopsy. By combining PET/CT with 3D ultrasound images, multimodality image-guided targeted biopsy may be able to improve the detection of prostate cancer.

2 Multimodality Molecular Image-Guided Biopsy System

We focus on a PET/CT directed, 3D ultrasound-guided biopsy system (Fig. 1). The steps of targeted prostate biopsy are as follows. (1) Before undergoing prostate biopsy, the patient undergoes a PET/CT scan with FACBC as part of the examinations. The anatomic CT images will be combined with PET images for improved localization of the prostate and suspicious tumors. (2) During biopsy, 3D ultrasound images are acquired immediately before needle insertion. The 3D ultrasound images are registered with the PET/CT data for biopsy planning. Three-dimensional visualization tools guide the biopsy needle to a suspicious lesion. (3) At the end of each core biopsy, the needle tip position is recorded on the real-time ultrasound images. The location information of biopsy cores is saved and then restored in the re-biopsy procedure. This allows the physician to re-biopsy the same area for a follow-up examination. The location information of the biopsy cores can also be used to guide additional biopsy to different locations if the original biopsy was negative.

3 Automatic Segmentation of 3D Prostate Ultrasound Images

Many methods for semi-automatic or automatic segmentation of the prostate in TRUS images have been proposed. Active shape models (ASM) was proposed to segment the prostate [10]. Knoll et al. proposed a deformable segmentation model that uses one-dimensional wavelet transform as a multi-scale contour parameterization tool to constrain the shape of the prostate model [11].

Our proposed method consists of the training and application stages. Two training TRUS images were used for wavelet features training and ten patients are used to make a predefined model. The prostate boundaries have been manually defined by specialists. A prostate shape model is created based on the allowable models of shape variations and its

probability. This model is employed to modify the prostate boundaries. The prostate textures are locally captured by training the locally placed Wavelet-based support vector machines (W-SVMs). With integrating local texture features and geometrical data, W-SVMs can robustly differentiate the prostate tissue from the adjacent tissues. The trained W-SVMs are employed to tentatively label the respective voxels around the surface into prostate and non-prostate tissues based on their texture features from different Wavelet filters. Subsequently, after an affine transformation of the shape model to the pre-defined prostate region that optimally matches with the texture features of the prostate boundary, the surface of the model is driven to the boundary between the tentatively labeled prostate and non-prostate tissues based on defined weighting functions and labeled voxels.

TRUS image textures can provide important features for accurately defining the prostate, especially for the regions where prostate boundaries are not clear. Biorthogonal wavelets 1.3, 1.5, and 4.4 are employed to extract the texture features of the prostate. Designing biorthogonal wavelets allows more degrees of freedom comparing to orthogonal wavelets. One additional degree of freedom is the possibility to construct symmetric wavelet functions. A number of W-SVMs on different regions of the surface model are placed and trained to adaptively label the tissue based on its texture and location. Each W-SVM is composed of 5 wavelet filter banks, voxel coordinates, and a Kernel Support Vector Machine (KSVM).

The wavelet filters are employed to extract texture features from TRUS images, and the KSVM is used to nonlinearly classify the Wavelet texture features for tissue differentiation. Each W-SVM corresponds to an individual sub-region in order to characterize and differentiate image textures locally and adaptively. All W-SVMs are trained to differentiate the texture features around its corresponding sub-regions in the training set. The trained W-SVMs are employed to tentatively label each voxel into prostate and non-prostate tissues in the application stage. To find more accurate segmentation, the set of W-SVMs is trained and applied in 3 planes (sagittal, coronal, transverse). Three sets of 2-D Wavelet filters were located at three orthogonal planes and were trained in each plane. Therefore, each voxel was tentatively labeled in three planes as prostate or non-prostate voxel. Fig. 2 shows the algorithm flowchart of the segmentation method.

A prostate probability model was used for modifying the segmentation. To build the prostate model, ten segmented prostates were registered using an affine transformation. Other registration methods can also be used to register the prostate of different patients [12–14]. In this study, we used the registration approach that is based on the principal axis transformation. This method was chosen because of its computational properties, speed and simplicity. The prostate volume was translated and rotated with respect to each other. The principal axis transformation is known from the classical theory of rigid bodies. A rigid body is uniquely located by knowledge of the position of its center of mass and its orientation (rotation) with respect to its center of mass. The center of mass, inertia matrix, and principal axes can be determined for any rigid body. For simple geometric shapes, the principal axes coincide with the axes of symmetry. In general, an orthogonal coordinate system is set up with their origin at the center of mass. When computed in the principal axis coordinate system, the inertia matrix is diagonal. The basic parameters that were used for

registration of the prostate are the position of the center of mass and rotation of the prostate about the center of mass, and the lengths of the principle axes. These properties uniquely determine the location and geometry of the prostate in three-dimensional space. After overlaying these 10 registered volumes, a probability model was created for each voxel based on how many prostate models are labeled as a voxel of the prostate at that region.

4 Nonrigid Registration of TRUS and CT Images

Our non-rigid registration method includes three terms: (1) surface landmark matching, (2) internal landmark matching, (3) volume overlap matching. Let x_i^{CT} and y_i^{US} are surface landmarks of the prostate from the segmented CT and TRUS images, respectively, u_k^{CT} and v_l^{US} are internal landmarks e.g. urethra and calcification within the prostate on the CT and TRUS images, respectively. B_{CT} and B_{US} represent the bladder neck region on the CT and TRUS images, respectively.

Inspired by [16–18], we design an overall similarity function to integrate the similarities between same type of landmarks and add smoothness constraints on the estimated transformation between segmented CT and TRUS images. The transformation between CT and TRUS images are represented by a general function, which can be modeled by various function basis. In our study, we choose B-splines as the transformation basis. The similarity function is written as:

$$E(f)=\alpha E_{SS}(f\{x_i^{CT},y_j^{US}\})+\beta E_{IS}(f\{u_k^{CT},v_l^{US}\})+\gamma E_{VM}(f\{B_{CT},B_{US}\})+\lambda E_S(f)$$

Where

$$E_{SS}(f)=\sum_{i=1}^{I}\sum_{j=1}^{J}p_{ij}(\|y_j^{US}-f(x_i^{CT})\|^2)+\delta\sum_{i=1}^{I}\sum_{j=1}^{J}p_{ij}\log(p_{ij})-\xi\sum_{i=1}^{I}\sum_{j=1}^{J}p_{ij}$$

$$E_{IS}(f)=\sum_{k=1}^{K}\sum_{l=1}^{L}q_{kl}\|v_l^{US}-f(u_k^{CT})\|^2+\tau\sum_{k=1}^{K}\sum_{l=1}^{L}q_{kl}\log(q_{kl})-\eta\sum_{k=1}^{K}\sum_{l=1}^{L}q_{kl}$$

$$E_{VM}(f)=1-\frac{2*(f(B_{CT})\cap B_{US})}{\left|f(B_{CT})\right|+\left|B_{US}\right|}$$

$$E_S(f)=\|\iiint_{(x,y,z)\in\Omega_M}\left(\frac{\partial^2 f}{\partial x^2}+\frac{\partial^2 f}{\partial y^2}+\frac{\partial^2 f}{\partial z^2}\right)^2 dxdydz\|^2$$

α, β, γ, and λ are the weights for each energy term. E_{SS} is the similarity for surface landmarks, and E_{IS} is the similarity for internal landmarks. E_{VM} is the energy term for the bladder-neck volume matching; and E_S is the smoothness constraint term. δ and τ are called the temperature parameter and its weighted term is an entropy term comes from the deterministic annealing technique [28]. ξ and η are the weight for the outlier rejection term. Matrixes p_{ij} and q_{kl} are the fuzzy correspondence matrixes [25]. f denotes the transformation between CT and TRUS images, which is B-spline transformation in our method.

The overall similarity function can be minimized by an alternating optimization algorithm that successively updates the correspondences matrixes p_{ij} and q_{kl}, and the transformation

function *f*. First, with the fixed transformation *f*, the correspondence matrixes between landmarks are updated by minimizing *E*(*f*). The updated correspondence matrixes are then treated as the temporary correspondences between landmarks. Second, with the fixed temporary correspondence matrixes p_{ij} and q_{kl}, the transformation function *f* is updated. The two steps are alternatively repeated until there are no updates of the correspondence matrixes.

5 Results

We developed a 3D ultrasound-guided biopsy system for the prostate. The system uses: (1) Passive mechanical components for guiding, tracking, and stabilizing the position of a commercially available, end-firing, transrectal ultrasound probe; (2) Software components for acquiring, storing, and reconstructing real- time, a series of 2D TRUS images into a 3D image; and (3) Software that displays a model of the 3D scene to guide a biopsy needle in three dimensions. The system allows real-time tracking and recording of the 3D position and orientation of the biopsy needle as a physician manipulates the ultrasound transducer.

The segmentation method was evaluated by five patient data sets of 3-D TRUS. Fig. 3 shows sample segmentation and its comparison with the corresponding gold standard. Quantitative performance assessment of the method was done by comparing the results with the corresponding gold standard data from manual segmentation. The Dice similarity and Sensitivity were used as performance assessment metrics in prostate classification algorithm. The numerical results of these evaluation criteria are shown in Table 1. The dice ratio is between 88.7%–95.0% among five prostate volumes. The mean and standard deviation of the dice function are 90.7% and 2.5%, respectively.

Fig. 4 shows the registration of ultrasound and MR images of a prostate phantom. The registration works well in the phantom experiment. We also evaluated the registration method using five sets of pre- and post-biopsy TRUS data of the same patients. The size of TRUS data is 244×244×175 voxels and the spatial resolution is 0.38×0.38×0.39 mm^3. We used pre-biopsy images as the reference images and registered the post-biopsy images of the same patient. For five sets of patient data, the target registration error (TRE) was 0.88±0.16 mm and the maximum TRE is 1.08±0.21 mm.

6 Discussion and Conclusion

We developed a PET/CT directed, 3D ultrasound-guided biopsy system for the prostate. In order to include other imaging modality such as PET/CT into 3D ultrasound-guided biopsy, we developed a 3D non-rigid registration method that combines point-based registration and volume overlap matching methods. The registration method was evaluated for TRUS and MR images. The registration method was also used to register 3D TRUS images acquired at different time points and thus can be used for potential use in TRUS-guided prostate re-biopsy. Our next step is to apply this registration method to CT and TRUS images and then incorporate PET/CT images into ultrasound image-guided targeted biopsy of the prostate in human patients.

In order to build a 3D model of the prostate, a set of Wavelet-based support vector machines and a shape model are developed and evaluated for automatic segmentation of the prostate TRUS images. Wavelet transform was employed for prostate texture extraction. A probability prostate model was incorporated into the approach to improve the robustness of the segmentation. With the model, even if the prostate has diverse appearance in different parts and weak boundary near bladder or rectum, the method is able to produce a relatively accurate segmentation in 3-D TRUS images.

Acknowledgments

This research is supported in part by NIH grant R01CA156775 (PI: Fei), Coulter Translational Research Grant (PI: Fei), Georgia Cancer Coalition Distinguished Clinicians and Scientists Award (PI: Fei), Emory Molecular and Translational Imaging Center (NIH P50CA128301), SPORE in Head and Neck Cancer (NIH P50CA128613), and Atlanta Clinical and Translational Science Institute (ACTSI) that is supported by the PHS Grant UL1 RR025008 from the Clinical and Translational Science Award program.

References

1. Roehl KA, Antenor JA, Catalona WJ. Serial biopsy results in prostate cancer screening study. J Urol. 2002; 167(6):2435–2439. [PubMed: 11992052]
2. Jambor I, Borra R, Kemppainen J, Lepomäki V, Parkkola R, Dean K, Alanen K, Arponen E, Nurmi M, Aronen HJ, Minn H. Functional imaging of localized prostate cancer aggressiveness using 11C-acetate PET/CT and 1H-MR spectroscopy. J Nucl Med. 2010; 51(11):1676–1683. [PubMed: 20956477]
3. Carlani M, Mancino S, Bonanno E, Finazzi Agrò E, Simonetti G. Combined morphological, [1H]-MR spectroscopic and contrast-enhanced imaging of human prostate cancer with a 3-Tesla scanner: preliminary experience. Radiol Med. 2008; 113(5):670–688. [PubMed: 18493829]
4. Schöder H, Herrmann K, Gönen M, Hricak H, Eberhard S, Scardino P, Scher HI, Larson SM. 2-[18F]fluoro-2-deoxyglucose positron emission tomography for the detection of disease in patients with prostate-specific antigen relapse after radical prostatectomy. Clin Cancer Res. 2005; 11(13): 4761–4769. [PubMed: 16000572]
5. Schilling D, Schlemmer HP, Wagner PH, Böttcher P, Merseburger AS, Aschoff P, Bares R, Pfannenberg C, Ganswindt U, Corvin S, Stenzl A. Histological verification of 11C-choline-positron emission/computed tomography-positive lymph nodes in patients with biochemical failure after treatment for localized prostate cancer. BJU Int. 2008; 102(4):446–451. [PubMed: 18410442]
6. DeGrado TR, Coleman RE, Wang S, Baldwin SW, Orr MD, Robertson CN, Polascik TJ, Price D. Synthesis and evaluation of 18F-labeled choline as an oncologic tracer for positron emission tomography: initial findings in prostate cancer. Cancer Res. 2001; 61(1):110–117. [PubMed: 11196147]
7. Oyama N, Akino H, Kanamaru H, Suzuki Y, Muramoto S, Yonekura Y, Sadato N, Yamamoto K, Okada K. 11C-acetate PET imaging of prostate cancer. J Nucl Med. 2002; 43(2):181–186. [PubMed: 11850482]
8. Nuñez R, Macapinlac HA, Yeung HW, Akhurst T, Cai S, Osman I, Gonen M, Riedel E, Scher HI, Larson S. Combined 18F-FDG and 11C-methionine PET scans in patients with newly progressive metastatic prostate cancer. J Nucl Med. 2002; 43(1):46–55. [PubMed: 11801702]
9. Schuster DM, Votaw JR, Nieh PT, Yu W, Nye JA, Master V, Bowman FD, Issa MM, Goodman M. Initial experience with the radiotracer anti-1-amino-3-18F-fluorocyclobutane-1-carboxylic acid with PET/CT in prostate carcinoma. J Nucl Med. 2007; 48(1):56–63. [PubMed: 17204699]
10. Hodge AC, Fenster A, Downey DB, Ladak HM. Prostate boundary segmentation from ultrasound images using 2D active shape models: Optimisation and extension to 3D. Computer Methods and Programs in Biomedicine. 2006; 84:99–113. [PubMed: 16930764]
11. Knoll C, Alcaniz M, Grau V, Monserrat C, Juan MC. Outlining of the prostate using snakes with shape restrictions based on the wavelet transform. Pattern Recognit. 1999; 32:1767–1781.

12. Fei B, Duerk JL, Sodee DB, Wilson DL. Semiautomatic nonrigid registration for the prostate and pelvic MR volumes. Academic Radiology. 2005; 12:815–824. [PubMed: 16039535]
13. Fei B, Lee Z, Duerk JL, Lewin JS, Sodee DB, Wilson DL. Registration and Fusion of SPECT, High Resolution MRI, and interventional MRI for Thermal Ablation of the Prostate Cancer. IEEE Transactions on Nuclear Science. 2004; 51(1):177–183.
14. Yang X, Akbari H, Halig L, Fei B. 3D non-rigid registration using surface and local salient features for transrectal ultrasound image-guided prostate biopsy. Proc SPIE. 2011; 7964
15. Alpert NM, Bradshaw JF, Kennedy D, Correia JA. The principal axes transformation a method for image registration. The Journal of Nuclear Medicine. 1990; 31(10):1717–1722. [PubMed: 2213197]
16. Chui H, Rangarajan A. A new point matching algorithm for non-rigid registration. Computer Vision and Image Understanding. 2002; 89(2–3):114–141.
17. Zhan Y, Ou Y, Feldman M, Tomaszeweski J, Davatzikos C, Shen D. Registering histologic and MR images of prostate for image-based cancer detection. Acad Radiol. 2007; 14:1367–1381. [PubMed: 17964460]
18. Yang J, Blum RS, Williams JP, Sun Y, Xu C. Non-rigid Image Registration Using Geometric Features and Local Salient Region Features. CVPR. 2006:1825–1832.

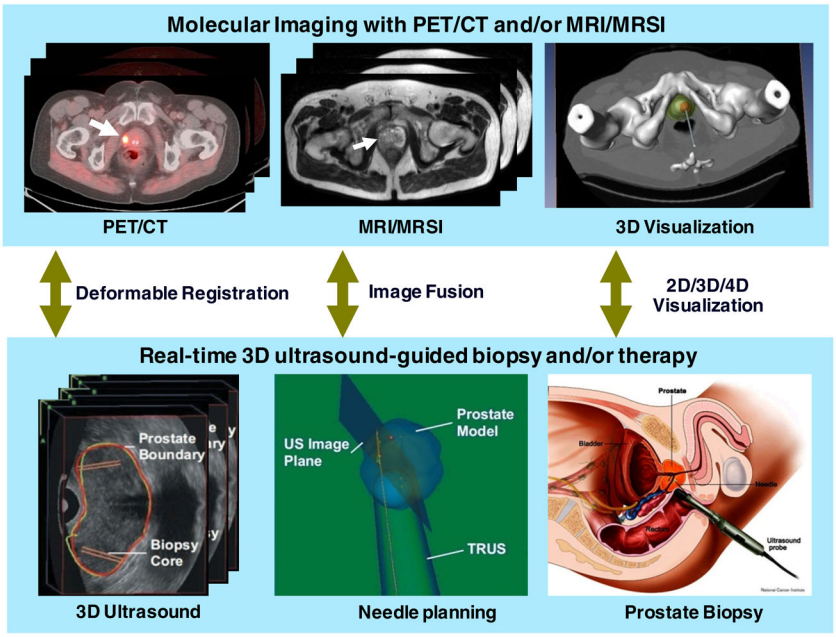

Fig. 1.

Molecular image-directed, ultrasound-guided system for targeted biopsy. *Top:* The PET/CT and MRI/MRS were acquired from the same patient at our institution. PET/CT with FACBC shows a focal lesion within the prostate (white arrow). MR images also show the suspicious lesion in the gland. The 3D visualization of the pelvis and prostate can aid the insertion of the biopsy needle into a suspicious tumor target. *Bottom:* A mechanically assisted navigation device was developed to acquire 3D TRUS images from the patient. The prostate boundaries are segmented from each slice and are then used to generate a 3D model of the prostate. Real-time TRUS images are acquired and registered to the 3D model in order to guide the biopsy. To incorporate PET/CT into ultrasound-guided procedures, deformable registration, segmentation, fusion, and visualization are the key technologies.

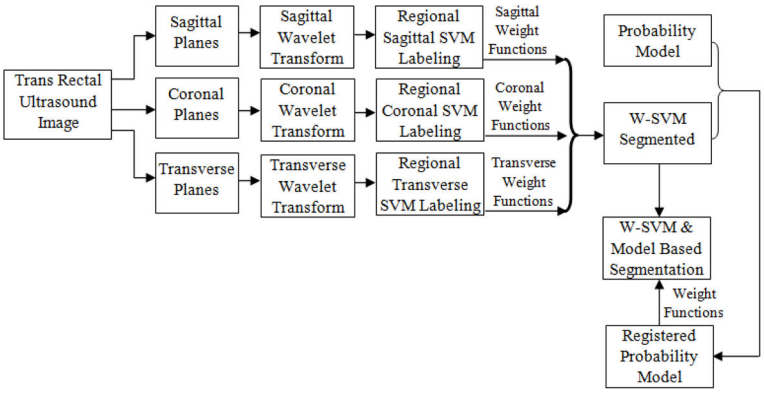

Fig. 2.
The flowchart of the wavelet-based segmentation algorithm

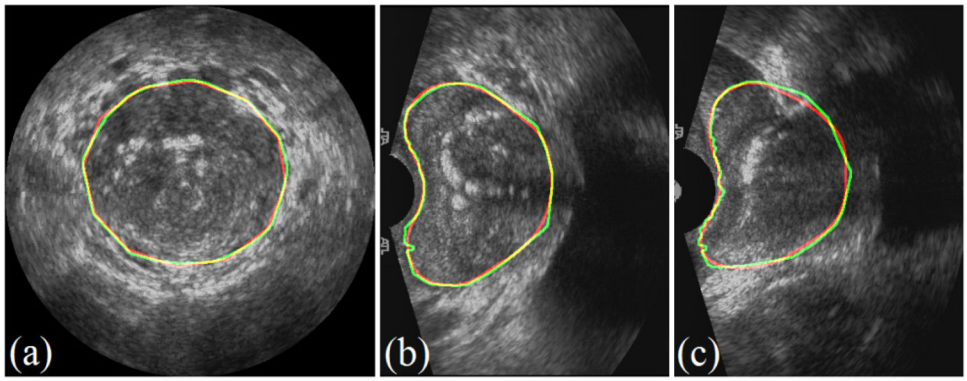

Fig. 3.

2-D segmentation results in different planes: red lines are the gold standard boundaries and green lines are the segmentation boundaries. (a) Coronal plane (b) Sagittal plane (c) Transverse plane.

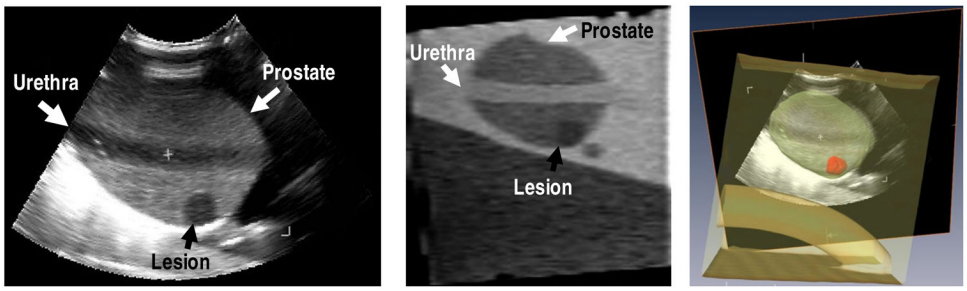

Fig. 4.

An ultrasound image (***l****eft*) is registered with an MR image (*middle*) of the same prostate phantom. The 3D visualization shows the relative location of the ultrasound plane within the 3D MR image (*right*) where green is the prostate and red is the lesion.

Table 1

Quantitative evaluation results of the segmentation method

Patients	1	2	3	4	5	Mean	STD
DICE	90.2%	88.7%	88.9%	95.0%	90.8%	90.7%	2.5%
Sensitivity	91.2%	95.2%	82.3%	93.6%	91.1%	90.7%	4.9%